Journal of Biomechanics 147 (2023) 111434

Contents lists available at ScienceDirect

Journal of Biomechanics

journal homepage: www.elsevier.com/locate/jbiomech

Correlation of mineral density and elastic modulus of dog dentin using μ-CT and nanoindentation

Jason W. Soukup [a,*], Justin Jeffery [b], Sienna R. Drizin [a], Scott J. Hetzel [c], Donald S. Stone [d], Melih Eriten [e], Heidi-Lynn Ploeg [e,f], Corinne R. Henak [e,g]

[a] Department of Surgical Sciences, University of Wisconsin-Madison, School of Veterinary Medicine, Madison, WI, USA
[b] Carbone Cancer Center, University of Wisconsin-Madison, School of Medicine and Public Health, Madison, WI, USA
[c] Department of Biostatistics and Medical Informatics, University of Wisconsin-Madison, School of Medicine and Public Health, Madison, WI, USA
[d] Department of Materials Science and Engineering, University of Wisconsin-Madison, College of Engineering, Madison, WI, USA
[e] Department of Mechanical Engineering, University of Wisconsin-Madison, College of Engineering, Madison, WI, USA
[f] Department of Mechanics and Materials Engineering, Queen's University, Kingston, ON, Canada
[g] Department of Orthopedics and Rehabilitation, University of Wisconsin-Madison, School of Medicine and Public Health, Madison, WI, USA

ARTICLE INFO

Keywords:
Dentin
Microcomputed tomography
μ-CT
Nanoindentation
Elastic modulus
Elasticity-density relationship
Mineral density
ρ_{QCT}

ABSTRACT

This study sought to 1) investigate the spatial distribution of mineral density of dog dentin using μ-CT and 2) characterize the relationship between the elastic modulus and mineral density of dog dentin using nanoindentation and μ-CT. Maxillary canine teeth of 10 mature dogs were scanned with a μ-CT then sectioned in the transverse and vertical planes and tested using nanoindentation. Spatial distribution of mineral density and elastic modulus was quantified. Results demonstrated significant spatial variation in mineral density and elastic modulus. Mineral density and elastic modulus generally increased from the dentin-pulp interface to the dentino-enamel junction and from the crown base to the crown tip. Significant site dependent correlations between mineral density and elastic modulus were determined ($0.021 > R^2 > 0.408$). The results of this study suggest that while mineral density is a mediator of elastic modulus, other mediators such as collagen content may contribute to the mechanical behavior of dog dentin.

1. Introduction

The tooth is a functional biocomposite composed primarily of two hierarchical, mineralized tissues: enamel and dentin. Dentin, with its heterogeneous arrangement of dentinal tubules within a matrix of hydroxyapatite crystals, supports the overlying enamel and contributes to distribution of stress and dissipation of crack energy from the enamel into dentin (Nanci, 2013). Dentinal tubules vary in diameter, with wider tubules at the dentin-pulp interface (DPI) than at the dentinoenamel junction (DEJ). (Hernández et al., 2010; Robb et al., 2007). Although dentin contributes to impressive failure resistance, excessive mechanical loading can cause failure especially when micro- and macro-structure is altered. Thus, better understanding tissue structure is a necessary step in modeling, predicting and understanding failure.

Computational models provide a mechanism to accurately model biological tissues with complex morphology and can elucidate the influence of structural and mechanical features of failure behavior across scales. While prior modeling efforts have proven useful in determining stress distribution within teeth and improved our understanding of dental mechanics, most models failed to account for material and structural heterogeneity and anisotropy (da Silva et al., 2013; Hubsch et al., 2002; Jiang et al., 2018; Maceri et al., 2009; Matson et al., 2012; Vilela et al., 2019). Material heterogeneity and anisotropy is expected to provide more accurate results and therefore higher clinical relevancy, particularly when considering patient-specific modeling (Thiagarajan et al., 2017). Similarly, site-dependent variability in mineral density has been observed in human molar dentin (Clementino-Luedemann & Kunzelmann, 2006). Quantifying the mineral density gradient throughout the entire volume will improve our understanding of dentin heterogeneity as it relates to material properties. Determining heterogeneous and patient-specific material behavior requires a three-dimensional understanding of mechanical properties and how they correlate with tissue mineral density.

Correlating tissue structure with functional material properties to

* Corresponding author.
E-mail address: jason.soukup@wisc.edu (J.W. Soukup).

https://doi.org/10.1016/j.jbiomech.2023.111434
Accepted 3 January 2023
Available online 7 January 2023

inform patient-specific diagnoses and treatment strategies is a focus of basic and medical research. Decreases in x-ray attenuation coefficient in carious dentin are highly correlated to decreases in mineral density (Angker et al., 2004; Neves Ade et al., 2010). Our previous work demonstrated poor to moderate relationships between dentin mechanical properties and tissue microstructure (Soukup et al., 2022).This suggests that other material tissue phases, such as mineral density, may contribute to elastic behavior more than tissue microstructure. Similarly, there is a strong correlation between mineral density and elastic modulus (E) in human carious dentin (Djomehri et al., 2015). In addition, mineral density is understood to be a key driver of mechanical behavior (Djomehri et al., 2015). Thus, volumetric mapping of mineral density in dentin is an important step in appreciating both tissue anisotropy and mechanical behavior.

Computed tomography (CT) provides a convenient mechanism to establish meaningful correlations between mineral density and mechanical properties. Empirical relationships between CT-acquired x-ray attenuation coefficient, mineral density and tissue mechanical properties enable the prediction of mechanical properties in a patient-specific, non-destructive way (Helgason et al., 2008; Schreiber et al., 2011). Over the last 3 decades, substantial work has been produced evaluating the relationships between elastic modulus and mineral density (elasticity-density relationship) in cortical and trabecular bone (Helgason et al., 2008; Knowles et al., 2016; Wirtz et al., 2000). Developing elasticity-density relationships requires an understanding of various definitions of density (Table 1): equivalent radiological density (ρ_{QCT}), ash density (ρ_{ash}), and apparent density (ρ_{app}). Elasticity-density relationships in bone, and their accuracy, vary, with a near ten-fold inter-study difference in predicted elastic modulus from cancellous bone density (Helgason et al., 2008; Knowles et al., 2016; Wirtz et al., 2000) (Linde et al., 1992). This large scatter may be due partly to the complexity of the experimental techniques and partly to the structural complexity of the tissue evaluated (Helgason et al., 2008). Nevertheless, establishing and refining these relationships in bone remain of significant interest. Investigations into the elasticity-density relationships in dental tissue are similarly of interest but have been minimally explored.

Given that, like bone, dentin is a three-phase composite material, techniques used in bone to establish a relationship between mineral density and elastic modulus should prove useful. To our knowledge, elasticity-density relationships in healthy dentin have not yet been established. Therefore, the aims of this study were to: 1) Investigate the spatial distribution of ρ_{QCT} (as a CT-calibrated measure of mineral density) of dog dentin using μ-CT and 2) Characterize the relationship between the elastic modulus and ρ_{QCT} of dog dentin using nanoindentation and μ-CT, thereby providing a non-destructive method for elastic modulus estimation. We hypothesize that 1) there is a mineral gradient present in dog dentin with mineral density increasing from the DPI to the DEJ and 2) the elastic modulus of dog dentin is significantly and strongly correlated to mineral density.

2. Methods

2.1. Sample acquisition

Ten maxillary canine teeth, used in a previous study (Soukup et al., 2022), were extracted from individual dogs after euthanasia for reasons unrelated to the study (Table 2). Sample size was determined based on practical implications and example studies from the literature (Helgason et al., 2008; Knowles et al., 2016). Teeth were wrapped in gauze saturated with Hanks' balanced salt solution, vacuum sealed and stored at −20 °C. Teeth were thawed at ambient temperature for 24 h prior to complete imbedding in a self-curing epoxy resin to create a tooth block (Fig. 1), which were allowed to cure in a vent hood for 24 h.

2.2. μ-CT acquisition and reconstruction

Tooth blocks were scanned with a Siemens Inveon μ-CT (Siemens Medical Solutions USA, Inc., Knoxville, TN). All scans were acquired with the following parameters: 80 kVp, 1000 μA current, 850 ms exposure time, 220 rotation steps with 500 projections, medium-high magnification, and binning factor of 2 using a 0.5 mm aluminum filter (to reduce beam hardening artifacts) (Verdelis & Salmon, 2019). Raw data were reconstructed with filtered back-projection applying the Shepp-Logan filter using the high-speed COBRA reconstruction software (Exxim Computing Corporation, Pleasanton, CA) yielding isotropic voxels of 39.7 μm. To further reduce the effects of beam hardening, all data were reconstructed with published coefficients (Mohapatra, 2012) represented by a third order polynomial.

2.3. Radiodensity

DICOM files for each of the ten teeth were imported into a dedicated medical imaging processing and analysis software program (Inveon Research Workplace; Siemens Medical). All samples were digitally sectioned according to their corresponding sections utilized for nanoindentation (Figs. 1 and 2). Specifically, five transverse μ-CT images and three vertical μ-CT images corresponding with transverse sections and vertical sections, respectively, were identified with a series of measurements in the software program. A detailed description of this process can be found in supplemental material. Subsequently, spatial distributions of radiodensity were evaluated. In each *transverse section,* 10 cuboid regions of interest (ROI) were manually delineated (five in the vestibulo-oral (VO) direction and five in the disto-mesial (DM) direction). In each *vertical section*, 6–12 cuboid ROIs were created from the crown base to the crown tip (Figs. 1 and 2). All ROIs corresponded to locations for nanoindentation evaluation. The mean ROIs size was 1550 voxels. In each ROI, the mean, median and variance of radiodensity in Hounsfield units (HU) were obtained.

Table 1
Definitions of common densitometric methods used in determining elasticity-density relationships in mineralized tissues.

Term	Symbol	Definition
Equivalent radiological density	ρ_{QCT}	density from CT-acquired x-ray attenuation coefficient converting to mineral density utilizing a mineral density phantom (e.g., hydroxyapatite)
Ash density	ρ_{ash}	ash weight (acquired after burning off non-mineral tissue) divided by the volume of mineralized tissue
Apparent density	ρ_{app}	wet weight (including non-mineral tissue) divided by the total sample volume
Ash/Apparent density ratio	ρ_{ash}/ρ_{app}	Ratio of ash density to apparent density

Table 2
Breed, age and sex of dogs from which teeth included in the study were obtained. (F = female; M = male; FS = spayed female; MN = neutered male).

Breed	Age (yrs)	Weight (kg)	Sex
Border collie	3.8	19	FS
Labradoodle	11.6	34.7	MN
Labrador retriever	1.5	30	M
Labrador retriever	12.4	37	MN
Golden doodle	7.0	37.2	FS
Miniature pinscher	15.6	3.2	MN
Siberian husky	11.1	21.8	FS
Labradoodle	12.2	31.5	FS
Vizsla	11.7	23.6	MN
Labrador retriever	11.5	43	MN

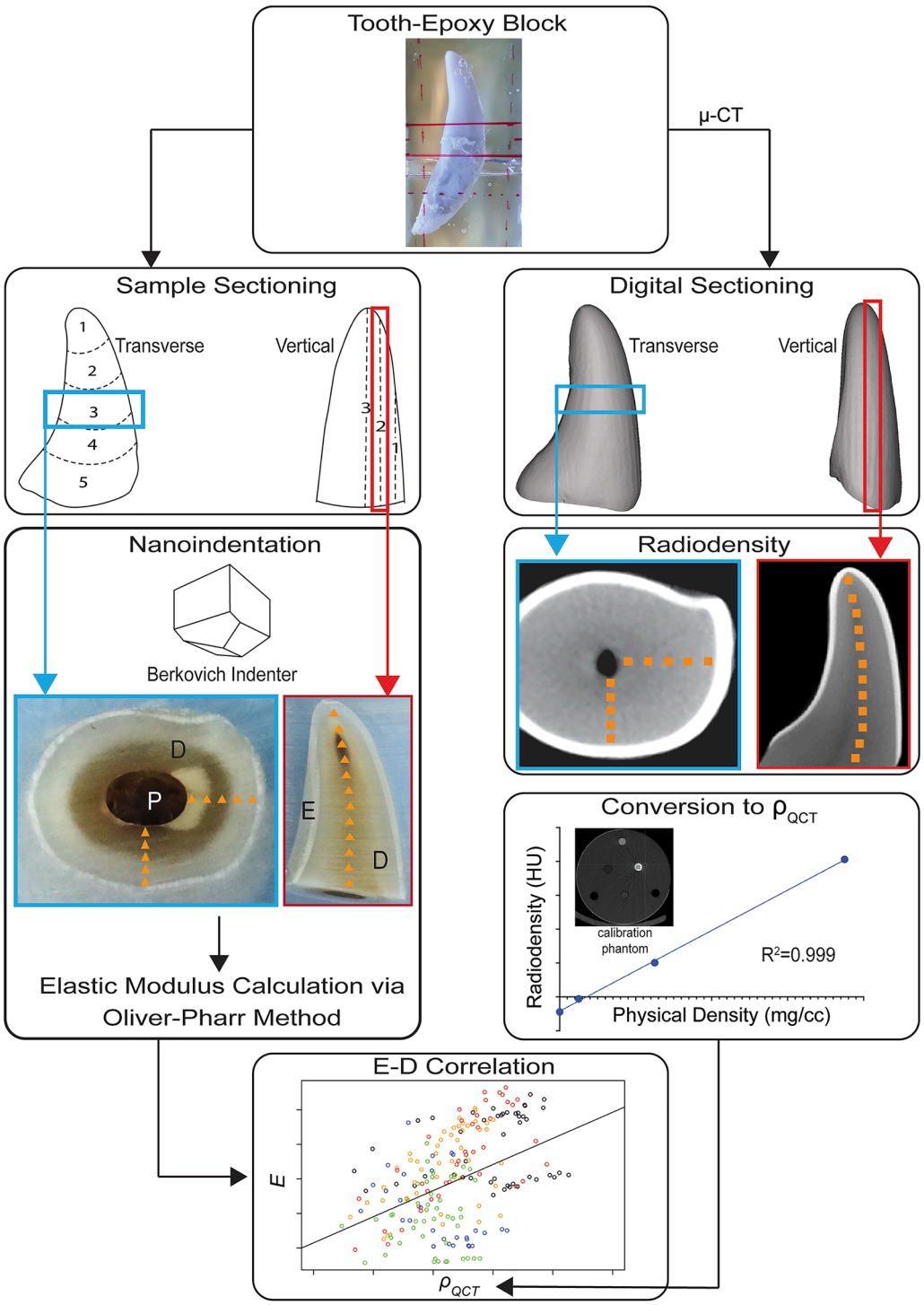

Fig. 1. Overview of experimental design. Blue boxes represent transverse sections and red boxes represent vertical sections. Orange triangles represent locations of nanoindentation data and orange squares represent ROIs for radiodensity measurement. P = pulp; D = dentin; E = enamel; E = elastic modulus; ρ_{QCT} = equivalent radiological density. (For interpretation of the references to color in this figure legend, the reader is referred to the web version of this article.)

2.4. μ-CT calibration and ρ_{QCT}

To counteract any instrument fluctuation between samples, one must calibrate radiological density measurements by measuring the CT scanner's response to a density calibration phantom. A calibration phantom containing four certified hydroxyapatite (HA) solution inserts of 0, 50, 250, and 750 mg/cc (Siemens Medical Solutions, Inc., Malvern, PA) was imaged with the same CT settings as the tooth samples. A 2.3 mm^3 cylindrical ROI was segmented in each HA insert at three separate locations (25%, 50% and 75% of insert length) and the mean radiodensity (HU) was recorded for each location. Regions of interest excluded the interface between HA and carrier material to avoid partial volume effects. The mean radiodensity (HU) of each HA insert was recorded and plotted against the HA mineral density (mg/cc). The resultant linear relationship (Fig. 3), defined by $\rho_{QCT} = m \times HU + intercept$, where m = slope, was used to convert radiological density at each tooth sample ROI to a calibrated measure of tissue mineral density; ***equivalent radiological density*** (ρ_{QCT}).

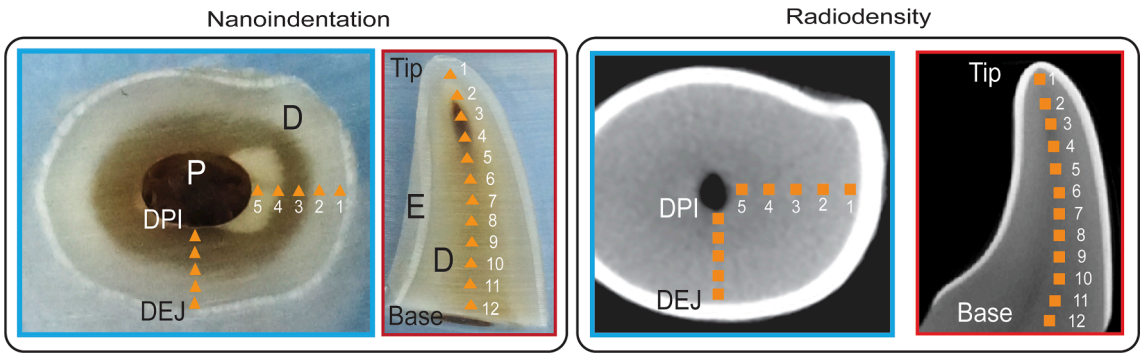

Fig. 2. Larger view of cross sections from Fig. 1 to show nanoindentation and radiodensity locations with numbering and orientations. Blue boxes represent transverse sections and red boxes represent vertical sections. Orange triangles represent locations of nanoindentation data and orange squares represent ROIs for radiodensity measurement. P = pulp; D = dentin; E = enamel; DEJ = dentino-enamel junction; DPI = dentin-pulp interface. (For interpretation of the references to color in this figure legend, the reader is referred to the web version of this article.)

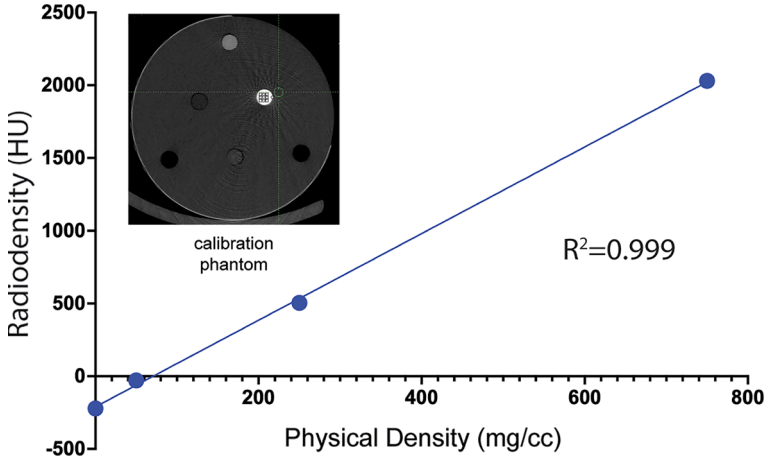

Fig. 3. Plot of linear regression model used to convert radiological density at each tooth sample ROI to ρ_{QCT}. Relationship is represented by y = 2.9769x – 210.47 (R^2 = 0.999).

2.5. Nanoindentation

Nanoindentation data were acquired for a previous study and the protocol for sectioning and testing was described in detail (Soukup et al., 2022). In brief, five teeth were sectioned with a Leica SP1600 high-precision, diamond histological saw into five transverse crown sections each. The crowns of the remaining 5 teeth were sectioned into three vertical crown sections each (Figs. 1 and 2). All sections were ground with 400, 600, 800 and 1200 grit silicon-carbide sandpaper on a water-cooled, low-speed benchtop grinder/polisher (Ecomet III, Beuhler, Lake Bluff, IL). Sequential polishing with 6, 1 and 0.25 μm diamond suspensions and a polishing cloth was then performed. Between polishings, all samples underwent a 1 min rinse with distilled water. Nanoindentation was performed in locations corresponding to the ROIs described above with a TI 950 Triboindenter (Bruker, Minneapolis, MN). (Figs. 1 and 2) All indentations were made with a TI-0083 high-load Berkovich indenter (Bruker, Minneapolis, MN) on a high-load transducer using a controlled displacement of 5000 nm with a 5 sec load and 5 sec unload time. Load and displacement were continuously recorded at 200 Hz. Load-displacement curves were used to derive elastic modulus using the Oliver-Pharr method (Oliver & Pharr, 1992, 2004).

2.6. Statistical analysis and elastic modulus-ρ_{QCT} correlation

The statistical assessment of correlation involved fitting linear mixed effects (LME) regression models with one variable of interest (elastic modulus) as the outcome and fixed effect predictor (ρ_{QCT}). Correlation was then estimated as the coefficient of determination (R^2) from the LME model. The assumed mirrored distribution pattern (based on understanding of microstructure) for elastic modulus in the transverse sections between the VO and DM directions was confirmed by the data. Subsequently, analogous positions in the VO and DM directions were combined for statistical analysis. Estimation of mean (95% CI) for each Section required fitting individual mixed effects ANOVA models with elastic modulus and ρ_{QCT} as the outcome, Section as a fixed factor variable, and Tooth as a random effect. A similar analysis method was used for estimating mean (95% CI) for each Position with Position as the fixed factor variable and the rest of the model structure staying the same. This process was done separately in both the transverse and vertical directions. If the ANOVA p-value was significant ($p < 0.05$) then two-way post-hoc analyses with Tukey's family-wise correction was used through the implementation of the emmeans function in R. A post hoc analysis was then performed to evaluate the effect of transverse position on the correlation. All analyses were conducted in R for statistical computing v4.0.

3. Results

3.1. ρ_{QCT}

ρ_{QCT} varied between 1.09 g/cc and 2.06 g/cc. As hypothesized, a mineral density gradient was seen in dog dentin with a decrease in ρ_{QCT} as a function of distance from the DEJ to the DPI (Fig. 4) and from the crown tip to the base (Fig. 5). Significant differences between sections

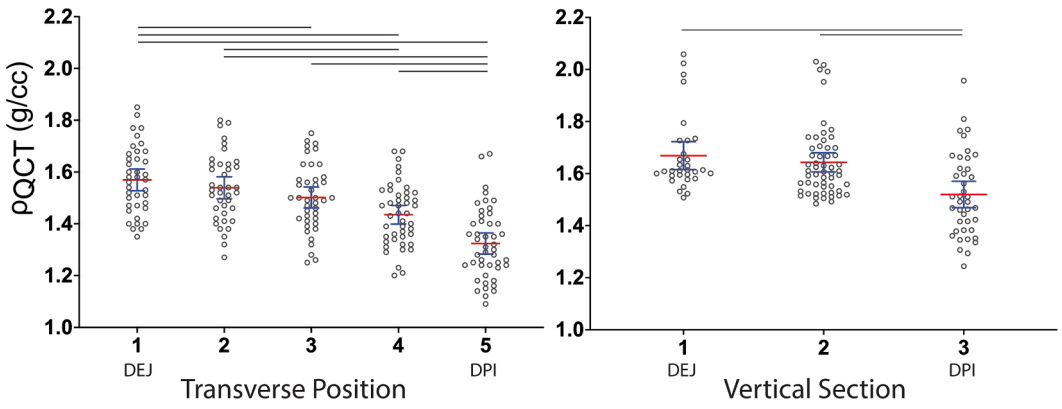

Fig. 4. Plots representing mineral density values in the transverse plane. Mean and 95% confidence intervals for ρ_{QCT} as a function of combined transverse positions (A) and vertical section (B). These plots show the mineral gradient with ρ_{QCT} decreasing from DEJ to DPI. Significance between positions and sections is noted with solid bars. In panel A, data points per position were. position 1, n = 39; position 2, n = 39; position 3, n = 41; position 4, n = 45; position 5, n = 46. For panel B, sections 1, 2 and 3 represent n = 31, n = 56 and n = 41, respectively.

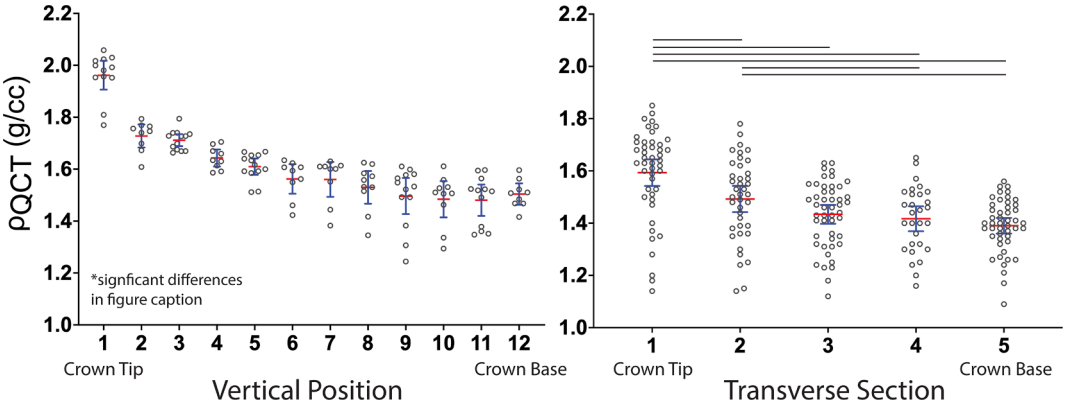

Fig. 5. Plots representing mineral density values in the vertical plane. Mean and 95% confidence intervals for ρ_{QCT} as a function of vertical position (A) and transverse section (B). These plots show the mineral gradient with ρ_{QCT} decreasing crown tip to crown base. Significance between sections is noted with solid black bars in B. Significant differences for vertical positions (A) are. 1 *vs* 2–12; 2 *vs* 5–12; 3 *vs* 6, 7, 9–12; 4 *vs* 9–12; and 5 *vs* 9–11. In panel A, data points per position were. position 1 and 11, n = 12; positions 2, 4, 6, 7 and 12, n = 9; position 3, 5 and 9n = 13; positions 8 and 10, n = 10. In panel B, each transverse section represents n = 50.

and positions were found in both transverse and vertical sections. A substantial decrease in ρ_{QCT} was visible near the DPI (Fig. 4) and a substantial increase in ρ_{QCT} was visible at the crown tip (Fig. 5).

3.2. Elastic modulus

Results of elastic modulus evaluation were previously published (Soukup 2022). To appreciate the elastic modulus gradient in dog dentin and the visual relationship between elastic modulus and ρ_{QCT} distributions, the spatial distribution of elastic modulus is described in brief here. Like ρ_{QCT}, elastic modulus decreased as a function of distance from the DEJ to the DPI and from the crown tip to crown base ($p < 0.001$).

3.3. Correlation between e and ρ_{QCT}

A visual relationship in the spatial distribution of elastic modulus and ρ_{QCT} can be appreciated (Figs. 4 and 5). In most specimens, a decrease in ρ_{QCT} consistently reflected a decrease in elastic modulus. In vertical sections elastic modulus increased from the DEJ to the DPI whereas ρ_{QCT} decreased (Soukup et al., 2022). The elastic modulus/ρ_{QCT} linear regression model yielded significant correlation when all (transverse and vertical) data points were considered together ($R^2 = 0.206$; $p < 0.001$). The correlation improved ($R^2 = 0.408$; $p < 0.001$) when the transverse section data was separated from the vertical section data. (Fig. 6) Correlation between elastic modulus and ρ_{QCT} for the vertical section data was also significant ($R^2 = 0.284$; $p < 0.001$). (Fig. 6) When the influence of volumetric location on the relationship between elastic modulus and ρ_{QCT} was considered, variance in the relationship was noted. (Figs. 7 and 8) Correlations between elastic modulus and ρ_{QCT} generally had steeper slopes and higher correlation coefficients closest to the DEJ.

4. Discussion

The aims of this study were to: 1) Investigate the spatial distribution of ρ_{QCT}, as a CT-calibrated measure of mineral density, of dog dentin using μ-CT and 2) Characterize the relationship between the elastic modulus and ρ_{QCT} of dog dentin using nanoindentation and μ-CT. Our stated hypotheses were 1) there is a mineral gradient present in dog dentin with mineral density increasing from the DPI to the DEJ and 2) the elastic modulus of dog dentin is significantly and strongly correlated to mineral density. μ-CT demonstrated that mineral density of dog dentin was spatially variable, providing confirmatory evidence for our first hypothesis. Dentin mineral density (1.09 g/cc to 2.06 g/cc) measured in this study is consistent with prior measures for human dentin (Clementino-Luedemann & Kunzelmann, 2006; Djomehri et al., 2015; Schwass et al., 2009). The spatial quantification, a novel contribution of this study, showed a mineral gradient throughout the dentin of

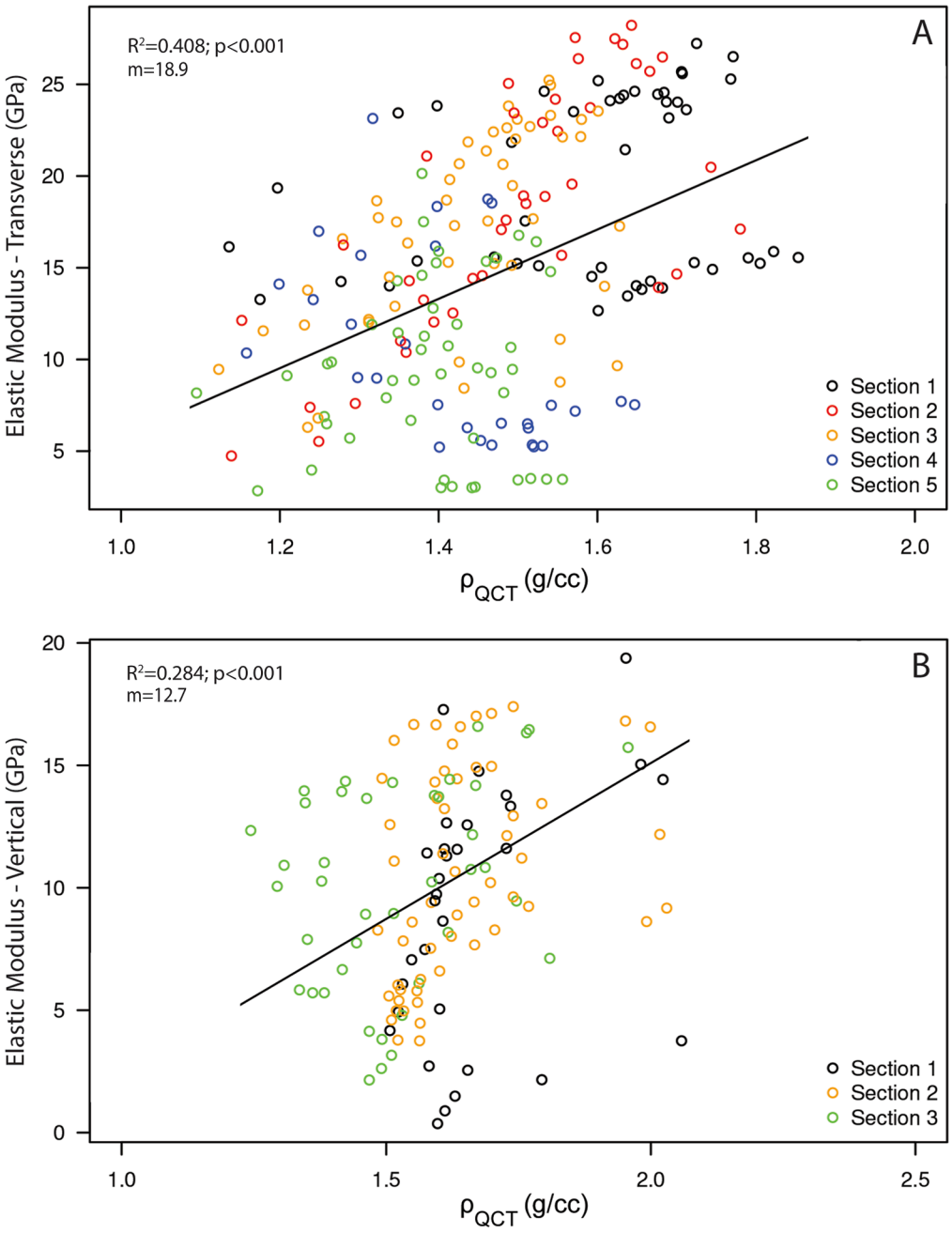

Fig. 6. Linear regression plots depicting the correlation between transverse section elastic modulus and ρ_{QCT} (A) and between vertical section elastic modulus and ρ_{QCT} (B). For plot A, individual transverse sections are color-coded; black circles = section 1 (crown tip), red circles = section 2, yellow circles = section 3, blue circles = section 4, green circles = section 5 (crown base). For plot B, individual vertical sections are color-coded; black circles = section 1 (near DEJ), green circles = section 2, red circles = section 3 (near DPI). m = slope. (For interpretation of the references to color in this figure legend, the reader is referred to the web version of this article.)

the dog canine tooth. This gradient is intuitive based on dentin microstructure: dentinal tubules radiate outward from the DPI to the DEJ within a matrix of mineralized tissue. Dentinal tubules measure approximately 3 μm in diameter near the DPI and decrease to approximately 2.4 μm at the DEJ (Lopes et al., 2009; Robb et al., 2007). We recently showed that the tubule density decreases as a function of distance from the DPI to the DEJ (Soukup et al., 2022). Thus, tubule content is maximized while mineral matrix is minimized near the DPI. Near the DEJ, tubule volume decreases and mineralized matrix volume increases. Additionally, the heterogeneity seen between the vertical and transverse sections was anticipated given that our previous work on microstructure and elastic modulus of dog dentin showed similar heterogeneity and anisotropy (Soukup et al., 2022).

While our results show that mineral density in dog dentin is consistent with measures of mineral density in human dentin, there are some notable differences. The upper and lower ends of the density range are higher than reported in human dentin (Clementino-Luedemann & Kunzelmann, 2006). The maximum mineral density values in our study were in the position nearest the DEJ in the vertical sections. An increase in mineral density near the DEJ would be anticipated based on previous work showing that this area is generally devoid of dentinal tubules. In addition, some evaluators have shown that some dentin regions in human teeth have hypermineralized areas (Angker et al., 2004). Such may be the case in dog dentin. Studies correlating our results with mineral content (i.e., calcium and phosphorus) may be warranted.

The relationship between ρ_{QCT} and elastic modulus was significant for transverse sections and when separated by distance from the DEJ, partially confirming our second hypothesis. Given the significant changes in tissue microstructure throughout the volume of dentin, it is reasonable to link this variation in correlation to the tissue microstructure. However, we previously showed that microstructure alone was not highly correlated with elastic modulus. Thus, further investigation into

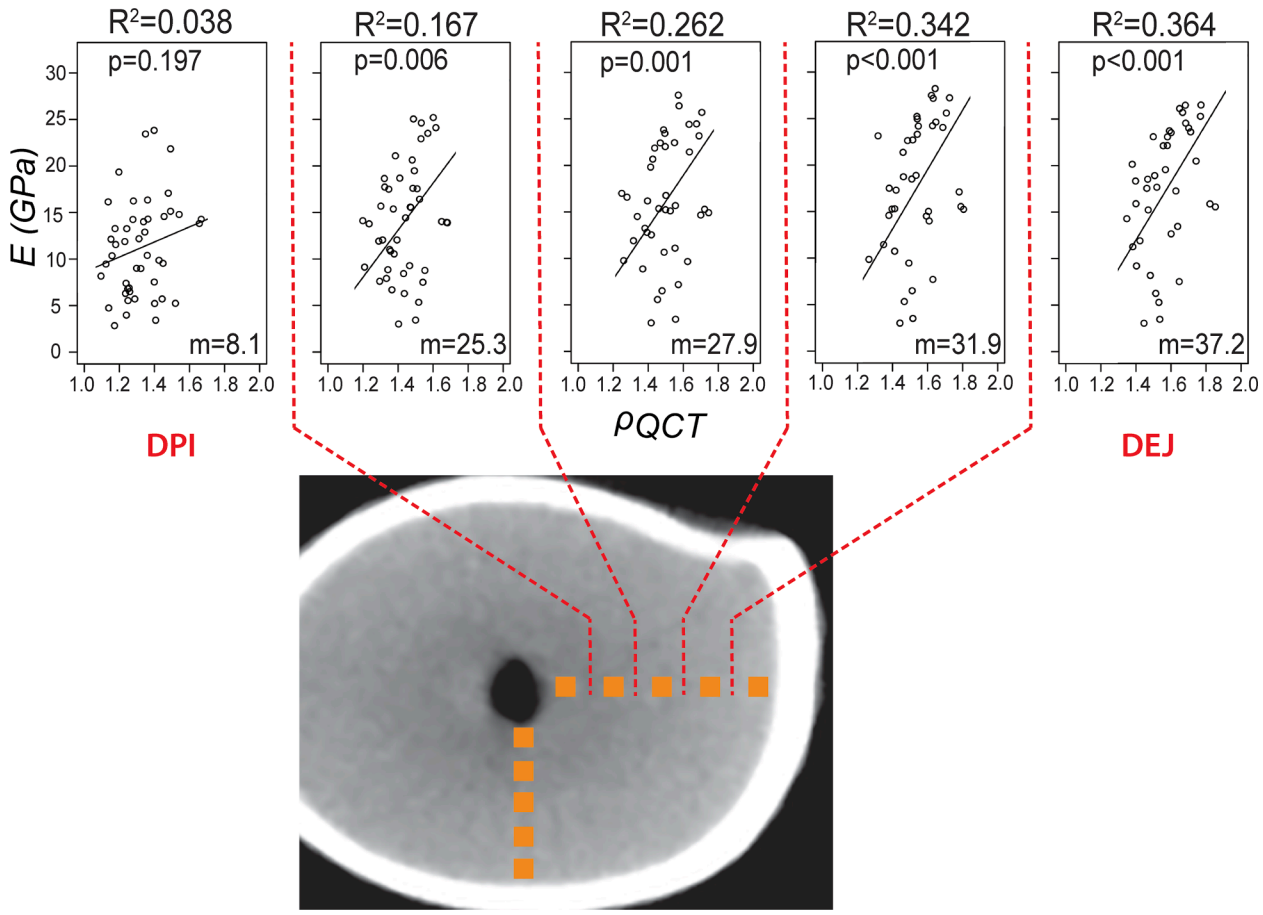

Fig. 7. Linear regression plots as a function of transverse position. Plots reveal the R^2 value improves, and the slope (m) increases from the DPI to the DEJ.

the contribution of non-mineral, non-structural features of dentin such as collagen in mediating elastic behavior is warranted (Uniyal et al., 2022).

Our results showed moderate to poor correlation between ρ_{QCT} and elastic modulus in transverse and vertical sections, respectively, contrary to our second hypothesis. Prior research has evaluated correlations between mechanical properties and back-scattered electron (BSE) microscopy-acquired mineral content of carious human dentin (Angker et al., 2004). Decreases in hardness and elastic modulus were strongly correlated with a reduction in mineral content, consistent with the current study, but with larger correlation coefficients than in the current study ($R^2 = 0.8975$ for mineral content by weight, $R^2 = 0.8947$ for mineral content by volume). The difference in correlation between the current study and the prior study may be due to methodology (BSE *vs* μ-CT) differences (Helgason et al., 2008). BSE can provide higher resolution than μ-CT, which may contribute to better correlation between elastic modulus and mineral density (Angker et al., 2004). In addition, the differences in estimates of mineral density between the BSE and μ-CT may lead to different correlations. Tissue microstructure differences between carious and healthy dentin would also be expected. The demineralization process in carious dentin preferentially attacks the hypermineralized peritubular dentin (Marshall, 1993). In addition, relative collagen content is higher. Thus, elasticity-density relationships in carious dentin may be mediated more by the less mineralized intertubular dentin and the collagen content relative to healthy dentin.

There are several factors that may have caused the poor to moderate correlation found in this study. Evaluation of the intra-site variation in elasticity-density relationships revealed that the correlation changes based on cross-section location within the dentin. Since differences in microstructural architecture between the DPI and the DEJ are significant in dog canine dentin (Soukup et al., 2022), these results suggest that intra-site variation in tissue microstructure may be enough to disrupt the correlation between ρ_{QCT} and elastic modulus. This would be consistent with elasticity-density relationships that vary in bone across anatomical site (e.g., vertebrae *vs* femur), which has been attributed to variations in tissue architecture (Morgan et al., 2003). This work, and our previous work (Soukup et al., 2022), suggests that intra-site variation in tissue architecture is a major consideration when developing elasticity-density relationships in dog dentin.

In addition, while mineral density was shown to decrease from the DEJ to the DPI, our previous work revealed an increase in elastic modulus from the DEJ to the DPI in vertical sections (Soukup et al., 2022). This contributed to a lack of good correlation in the vertical sections. The cause for the pattern of increasing elastic modulus from DEJ to DPI was unexpected and not easily accounted for. It is possible that, due to the complex structure of dentin (e.g., sigmoid dentinal tubule path, variation in peritubular dentin content, etc.), indentations were performed in samples with varying microstructure which would have profoundly affected the elastic modulus and may have contributed to imperfect elastic modulus measurements.

Another factor that may have impacted our results is the use of a polychromatic radiation source. Bench-top μ-CT systems utilize polychromatic radiation, which results in attenuation that is the summation of both mineral and organic phases (Djomehri et al., 2015). While it is likely that the organic phase of dentin is small enough that the contribution to the ρ_{QCT} result is negligible, perhaps using a monochromatic source of radiation (i.e., synchrotron) would improve the correlations between ρ_{QCT} and elastic modulus.

In addition, the density used to define mineral density can influence results. While we used ρ_{QCT}, the literature on bone suggests that ρ_{ash} or

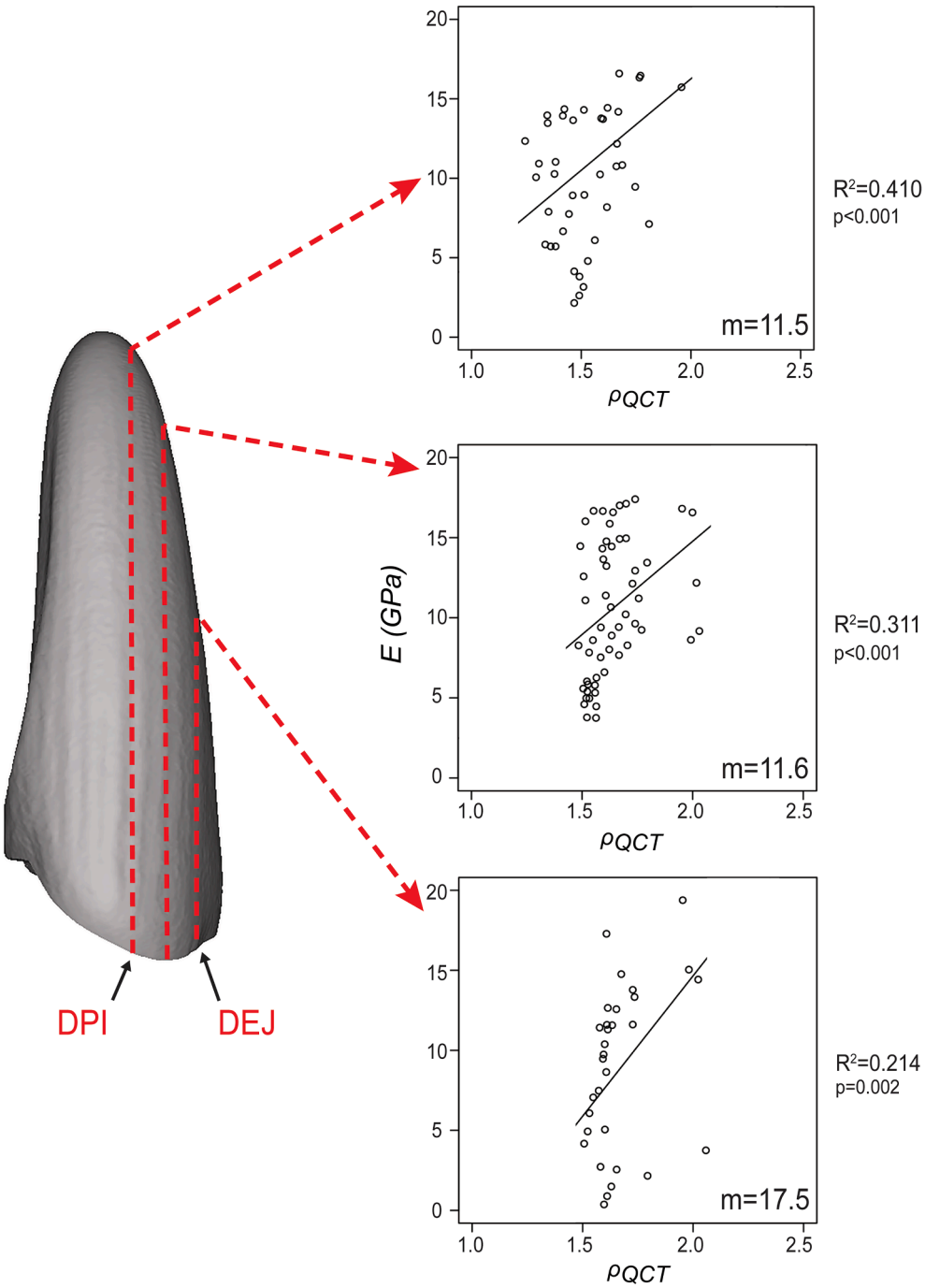

Fig. 8. Linear regression plots as a function of vertical section. Plots reveal the R^2 value improves, and the slope (m) decreases from the DEJ to the DPI.

ρ_{app} provides the most accurate elastic-density relationships (Aiyangar et al., 2014; Helgason et al., 2008). Correlations between material properties and ρ_{ash} or ρ_{app} generally follow a power law relationship, but the relationships between properties and ρ_{QCT} were linear in this study. While relationships are established for bone, those between dentin ρ_{QCT} and ρ_{ash} have not been established. In human vertebral and femoral bone, ρ_{QCT} is highly correlated with ρ_{ash}, thus our assumption that ρ_{QCT} would be a meaningful measure of mineral density (Aiyangar et al., 2014; Schileo et al., 2008). Further, directly acquiring ρ_{ash} and/or ρ_{app} requires tissue destruction and is technically challenging. Given the microstructural gradient previously shown in dentin (Soukup et al., 2022) and the mineral gradient shown here, the establishment of a linear relationship between ρ_{ash} and ρ_{QCT} would require sampling small dentin tissue throughout the entire volume of the tooth, which would be technically demanding. Nevertheless, future efforts to correlate dentin ρ_{ash} with ρ_{QCT} should be made, particularly in light of our results.

Various dog breeds and sexes were used in this study, both of which are known to have an influence on canine tooth size (Gittleman and van Valkenburgh, 1997). Although unanswerable within the limitations of the experimental design and data set, it is interesting to ponder what effect, if any, sexual dimorphism or dog/tooth size may have on any elasticity-density correlations. There is no evidence that sexual dimorphism alone has effect on elasticity-density relationships in mineralized tissues.

Several inherent limitations in measuring dentin mineral density for μ-CT were present and may have limited our ability to acquire strong correlation between ρ_{QCT} and elastic modulus. Although we corrected for beam hardening, it cannot be completely removed from the

polychromatic radiation source utilized in bench-top μ-CT systems. Complete removal of beam hardening requires the use of a monochromatic radiation source, which have inherent accessibility issues. To avoid partial volume effects, all ROIs used for mineral density acquisition were kept at least several pixels away from the enamel. However, it is possible that the volumetric nature of the ROI may have allowed an edge of the ROI cube to come close enough to the dentin-enamel interface such that mineral density may have been artificially increased.

Some error in recreating nanoindentation position in digital sections was anticipated. Physical transverse and vertical tooth sections were created with a precision histological saw with a kerf of 300 μm. Assuming that the digital section was taken exactly at the midpoint of the saw kerf, the transverse digital sections may be offset by approximately 150 μm in the vertical direction. Similar errors would be expected in the vertical digital sections. This would be the largest source of error and one that should be corrected in future experiments.

5. Conclusions

Our results show that the mineral density of dog dentin is heterogeneous. In addition, a mineral gradient is present that is consistent with reports in human dentin and consistent with the dentin microstructure. Dentin mechanical properties and ρ_{QCT} are moderately correlated with the best correlations found in data from transverse cross sections. It is possible that the changes in tissue microstructure throughout the volume of the dentin contribute to intra-site variation. Continued efforts should be made to investigate other possible mediators of dentin material properties.

Author contributions

All authors of this work have made substantial contributions to all the following: (1) the conception and design of the study, or acquisition of data, or analysis and interpretation of data, (2) drafting the article or revising it critically for important intellectual content and (3) final approval of the version to be submitted.

CRediT authorship contribution statement

Jason W. Soukup: Writing – review & editing, Writing – original draft, Visualization, Validation, Software, Methodology, Investigation, Formal analysis, Data curation, Conceptualization. **Justin Jeffery:** Writing – review & editing, Writing – original draft, Methodology. **Sienna R. Drizin:** Writing – review & editing, Investigation. **Scott J. Hetzel:** Writing – review & editing, Writing – original draft, Formal analysis, Data curation. **Donald S. Stone:** Writing – review & editing, Supervision, Methodology. **Melih Eriten:** Writing – review & editing, Supervision, Methodology. **Heidi-Lynn Ploeg:** Writing – review & editing, Supervision, Resources, Methodology, Conceptualization. **Corinne R. Henak:** Writing – review & editing, Writing – original draft, Supervision, Resources, Project administration, Methodology, Formal analysis, Data curation, Conceptualization.

Declaration of Competing Interest

The authors declare that they have no known competing financial interests or personal relationships that could have appeared to influence the work reported in this paper.

Acknowledgements and Funding

This project was supported by funding from the Institutional Clinical and Translational Science Award UL1 TR002373 and by the University of Wisconsin Carbone Cancer Center Support Grants P30 CA014520 and NCI P30 CA014520. The authors gratefully acknowledge use of facilities and instrumentation at the UW-Madison Wisconsin Centers for Nanoscale Technology partially supported by the NSF through the University of Wisconsin Materials Research Science and Engineering Center Grant DMR-1720415. We would like to thank and acknowledge the intellectual and technical contributions of the UW-Madison Small Animal Imaging and Radiotherapy Facility; and Richard Noll and Dr. Julie Morasch of the UW-Madison Wisconsin Centers for Nanoscale Technology. In addition, we would like to thank Dr. Caitlin Collins for her early support and inspiration.

Appendix A. Supplementary data

Supplementary data to this article can be found online at https://doi.org/10.1016/j.jbiomech.2023.111434.

References

Aiyangar, A.K., Vivanco, J., Au, A.G., Anderson, P.A., Smith, E.L., Ploeg, H.L., 2014. Dependence of Anisotropy of Human Lumbar Vertebral Trabecular Bone on QCT-Based Apparent Density. J. Biomech. Eng. 136 (9), 091003 https://doi.org/10.1115/1.4027663.

Angker, L., Nockolds, C., Swain, M.V., Kilpatrick, N., 2004. Correlating the mechanical properties to the mineral content of carious dentine - A comparative study using an ultra-micro indentation system (UMIS) and SEM-BSE signals. Arch Oral Biol. 49 (5), 369–378. https://doi.org/10.1016/j.archoralbio.2003.12.005.

Clementino-Luedemann, T.N.R., Kunzelmann, K.H., 2006. Mineral concentration of natural human teeth by a commercial micro-CT. Dent. Mater. J. 25 (1), 113–119. https://doi.org/10.4012/dmj.25.113.

da Silva, B.R., Moreira Neto, J.J.S., da Silva, J.I., de Aguiar, A.S.W., 2013. Three-dimensional finite element analysis of the maxillary central incisor in two different situations of traumatic impact. Comput. Methods Biomech. Biomed. Eng. 16 (2), 158–164. https://doi.org/10.1080/10255842.2011.611115.

Djomehri, S.I., Candell, S., Case, T., Browning, A., Marshall, G.W., Yun, W., Lau, S.H., Webb, S., Ho, S.P., 2015. Mineral density volume gradients in normal and diseased human tissues. PLoS One 10 (4), 1–24. https://doi.org/10.1371/journal.pone.0121611.

Gittleman, J.L., van Valkenburgh, B., 1997. Sexual dimorphism in the canines and skulls of carnivores: effects of size, phylogency, and behavioural ecology. J. Zool. 242 (1), 97–117. https://doi.org/10.1111/j.1469-7998.1997.tb02932.x.

Helgason, B., Perilli, E., Schileo, E., Taddei, F., Brynjólfsson, S., Viceconti, M., 2008. Mathematical relationships between bone density and mechanical properties: a literature review. Clin. Biomech. (Bristol, Avon) 23 (2), 135–146. https://doi.org/10.1016/j.clinbiomech.2007.08.024.

Hernández, S.Z., Negro, V.B., Paulero, R.H., Toriggia, P.G., Saccomanno, D.M., 2010. Scanning electron microscopy of pulp cavity dentin in dogs. J. Vet. Dent. 27 (1), 7–11.

Hubsch, P., Middleton, J., Knox, J., 2002. The influence of cavity shape on the stresses in composite dental restorations: A finite element study. Comput. Methods Biomech. Biomed. Eng. 5 (5), 343–349. https://doi.org/10.1080/1025584021000016861.

Jiang, Q., Huang, Y., Tu, X.R., Li, Z., He, Y., Yang, X., 2018. Biomechanical Properties of First Maxillary Molars with Different Endodontic Cavities: A Finite Element Analysis. J. Endod. 44 (8), 1283–1288. https://doi.org/10.1016/j.joen.2018.04.004.

Knowles, N.K., Reeves, J.M., Ferreira, L.M., 2016. Quantitative Computed Tomography (QCT) derived Bone Mineral Density (BMD) in finite element studies: a review of the literature. J. Exp. Orthopaedics 3 (1). https://doi.org/10.1186/s40634-016-0072-2.

Linde, F., Hvid, I., Madsen, F., 1992. The effect of specimen geometry on the mechanical behaviour of trabecular bone specimens. J. Biomech. 25 (4), 359–368. https://doi.org/10.1016/0021-9290(92)90255-Y.

Lopes, M.B., Sinhoreti, M.A.C., Gonini Júnior, A., Consani, S., McCabe, J.F., 2009. Comparative study of tubular diameter and quantity for human and bovine dentin at different depths. Braz. Dent. J. 20 (4), 279–283. https://doi.org/10.1590/s0103-64402009000400003.

Maceri, F., Martignoni, M., Vairo, G., 2009. Optimal mechanical design of anatomical post-systems for endodontic restoration. Comput. Methods Biomech. Biomed. Eng. 12 (1), 59–71. https://doi.org/10.1080/10255840802164079.

Marshall, G.W.J., 1993. Dentin: microstructure and characterization. Quintessence Int 24 (9), 606–617.

Matson, M.R., Lewgoy, H.R., Barros Filho, D.A., Amore, R., Anido-Anido, A., Alonso, R.C. B., Carrilho, M.R.O., Anauate-Netto, C., 2012. Finite element analysis of stress distribution in intact and porcelain veneer restored teeth. Comput. Methods Biomech. Biomed. Eng. 15 (8), 795–800. https://doi.org/10.1080/10255842.2011.561013.

Mohapatra, S., 2012. Development and quantitative assessment of a beam hardening correction model for preclinical.

Morgan, E.F., Bayraktar, H.H., Keaveny, T.M., 2003. Trabecular bone modulus-density relationships depend on anatomic site. J. Biomech. 36 (7), 897–904. https://doi.org/10.1016/S0021-9290(03)00071-X.

Nanci, A., 2013. Dentin-pulp complex. In: Nanci, A. (Ed.), Ten Cate's Oral Histology, 8th ed., Elsevier, pp. 165–204.

Neves Ade, A., Coutinho, E., Vivan Cardoso, M., Jaecques, S.V., Van Meerbeek, B., 2010. Micro-CT based quantitative evaluation of caries excavation. Dent Mater 26 (6), 579–588. https://doi.org/10.1016/j.dental.2010.01.012.

Oliver, W., Pharr, G., 1992. An improved technique for determining hardness and elastic modulus using load and displacement sensing indentation experiments. J Mater Res. 7, 1564–1583.

Oliver, W., Pharr, G., 2004. Measurement of hardness and elastic modulus by instrumented indentation: Advances in understanding and refinements to methodology. J. Mater. Res. 19 (01), 3–20. https://doi.org/10.1557/jmr.2004.19.1.3.

Robb, L., Marx, J., Steenkamp, G., Willie, F.P., Pretorius, E., Boy, S.C., 2007. Scanning Electron Microscopic Study of the Dentinal Tubules in Dog Canine Teeth. J Vet Dent 24 (2), 86–89. https://doi.org/10.1177/089875640702400203.

Schileo, E., Dall'ara, E., Taddei, F., Malandrino, A., Schotkamp, T., Baleani, M., Viceconti, M., 2008. An accurate estimation of bone density improves the accuracy of subject-specific finite element models. J Biomech 41 (11), 2483–2491. https://doi.org/10.1016/j.jbiomech.2008.05.017.

Schreiber, J.J., Anderson, P.A., Rosas, H.G., Buchholz, A.L., Au, A.G., 2011. Hounsfield units for assessing bone mineral density and strength: A tool for osteoporosis management. J. Bone Joint Surgery – Ser. A 93 (11), 1057–1063. https://doi.org/10.2106/JBJS.J.00160.

Schwass, D.R., Swain, M.V., Purton, D.G., Leichter, J.W., 2009. A system of calibrating microtomography for use in caries research. Caries Res 43 (4), 314–321. https://doi.org/10.1159/000226230.

Soukup, J.W., Hetzel, S.J., Stone, D.S., Eriten, M., Ploeg, H., Henak, C.R., 2022. Structure-function relationships in dog dentin. J. Biomech. 141 (July), 111218 https://doi.org/10.1016/j.jbiomech.2022.111218.

Thiagarajan, G., Vizcarra, B., Bodapudi, V., Reed, R., Seyedmahmoud, R., Wang, Y., Gorski, J.P., Walker, M.P., 2017. Stress analysis of irradiated human tooth enamel using finite element methods. Comput. Methods Biomech. Biomed. Eng. 20 (14), 1533–1542. https://doi.org/10.1080/10255842.2017.1383401.

Uniyal, P., Sihota, P., Kumar, N., 2022. Effect of organic matrix alteration on strain rate dependent mechanical behaviour of cortical bone. J. Mech. Behav. Biomed. Mater. 125 (September 2021), 104910 https://doi.org/10.1016/j.jmbbm.2021.104910.

Verdelis, K., Salmon, P., 2019. Microcomputed Tomography Imaging in Odontogenesis Studies. Methods Mol Biol. 1922, 309–324. https://doi.org/10.1007/978-1-4939-9012-2_28.

Vilela, A.B.F., Soares, P.B.F., Almeida, G.A., Veríssimo, C., Rodrigues, M.P., Versluis, A., Soares, C.J., 2019. Three-dimensional finite element stress analysis of teeth adjacent to a traumatized incisor. Dent. Traumatol. 35 (2), 128–134. https://doi.org/10.1111/edt.12453.

Wirtz, D.C., Schiffers, N., Forst, R., Pandorf, T., Weichert, D., Radermacher, K., 2000. Critical evaluation of known bone material properties to realize anisotropic FE-simulation of the proximal femur. J. Biomech. 33 (10), 1325–1330. https://doi.org/10.1016/S0021-9290(00)00069-5.